Domain-wall dynamics in a nanostrip with perpendicular magnetic anisotropy induced by perpendicular current injection

I. L. Kindiak,[1,2] P. N. Skirdkov,[2,3] K. A. Tikhomirova,[4] K. A. Zvezdin,[2,3]
E. G. Ekomasov,[5,6,7] and A. K. Zvezdin[3]

[1]*Moscow Institute of Physics and Technology, Institutskiy pereulok 9, 141700 Dolgoprudny, Russia*
[2]*New Spintronic Technologies, Russian Quantum Center, Bolshoy Bulvar 30, building 1, 121205 Moscow, Russia*
[3]*Prokhorov General Physics Institute of the Russian Academy of Sciences, Vavilova 38, 119991 Moscow, Russia*
[4]*Skolkovo Institute of Science and Technology, Skoltech, Building 3, 143026 Moscow, Russia*
[5]*University of Tyumen, Institute of Physics and Technology, Volodarskogo 6, 625003 Tyumen, Russia*
[6]*Bashkir State University, Institute of Physics and Technology, Zaki Validi 32, 450076 Ufa, Russia*
[7]*South Ural State University (National Research University), Laboratory of Functional Materials of the Scientific and Educational Center "Nanotechnology", Lenin Avenue 76, 454080 Chelyabinsk, Russia*

(Received 11 October 2019; revised 20 November 2020; accepted 11 January 2021; published 26 January 2021)

A numerical and analytical study of the dynamics of domain walls (DWs) in a magnetic tunnel junction with perpendicular magnetic anisotropy in a free layer is presented. Equilibrium states of the domain wall are obtained for various widths of the structure. The corresponding symmetries of the components of spin transfer torques $\mathbf{T}_{STT}$ and the polarizer directions favoring stable DW motion under perpendicular current injection are obtained. The DW steady motion with velocities up to 200 m/s at current densities below 10^6 A/cm^2 is reported. The Walker breakdown is demonstrated, and the dynamics of the postthreshold DW motion is investigated for various configurations of torques and polarizer directions. To have analytical insight into the investigated regimes of DW dynamics a theoretical model is developed and verified by micromagnetic simulations.

DOI: 10.1103/PhysRevB.103.024442

I. INTRODUCTION

Recently, studies of domain-wall (DW) dynamics in ferromagnetic nanowires have attracted much attention [1–5]. This is due to both purely fundamental interests and promising applications. Controlled DW dynamics can be used in spintronic devices such as racetrack memory [6], logic units [7–10], and spintronic memristors [11–13], which imitate neuronal synapses [14] and have great potential for use as the hardware basis of neuromorphic computational architectures. In this context, materials with perpendicular magnetic anisotropy (PMA) are of particular interest. Compared to materials with in-plane magnetic anisotropy, magnetic tunnel junctions (MTJs) with PMA [15–17] have attractive advantages, such as a lower critical excitation current, higher thermal stability [18–20], and a smaller DW width. Thus, PMA-based MTJs have the potential to be next-generation, energy-efficient, high-density spintronic devices.

Early DW-based spintronic device concepts required induced magnetic fields to control DW dynamics [1,21,22]. However, it was found that this approach is hardly suitable for close-packed arrays of nanoscale devices due to significant cross-talk effects. Spin-orbit torques (see the review in [23]) are another possible way to excite DW. Possible types of spin-orbit torque required for the excitation of steady DW motion for various anisotropy and DW types were first analyzed numerically in [24]. Such an approach of spin-orbit DW excitation was recently considered in detail for PMA materials [25–28]. In addition, spin-orbit coupling in ferromagnets can lead to the anomalous Hall effect and anisotropic magnetoresistance, which can also move the DW [29]. However, spin-orbit structures are more difficult to use to determine the position of a DW compared to magnetic tunnel junctions, with which it is possible to determine the position of a DW through the tunneling magnetoresistance. Thus, the spin-orbital torques, despite the higher efficiency of DW excitation, may be less attractive for neuromorphic and other real-life applications [14].

An alternative approach based on current-induced DW motion has been the subject of many experimental [2,4,30–32] and theoretical [33–37] studies. In these works, nanostructures were usually represented by a long and narrow magnetic nanostrip containing a DW. For this geometry, there are two possible current configurations: current in plane (CIP), when spin-polarized current flows in the plane of the magnetic film, and current perpendicular to the plane (CPP), when it flows perpendicular to the magnetic film surface. The CIP case was analyzed in detail for both planar and perpendicular magnetic anisotropies [38–41]. For the case of CPP geometry, it was demonstrated numerically [42] and experimentally [43,44] that the DW velocities can be up to two orders of magnitude higher than in the CIP configuration, provided that the current densities are equal. Thus, the CPP configuration requires relatively low current densities for efficient DW dynamics excitation [45,46]. The drawback of this configuration is the higher electric current required for efficient DW motion in a large cross-section area, which, however, can be addressed by using local current injection [47]. A detailed analytical

description of DW dynamics under the CPP injection with analysis of various polarizers was presented recently [48]. However, all these results correspond to the in-plane or even zero magnetic anisotropy, while the case of the CPP geometry in combination with the PMA ferromagnetic nanostrip remains unclear.

Based on the above arguments, perpendicular current injection seems to be the most efficient way of DW excitation, with the exception of spin-orbit torques, which, however, are limited by the difficulty of reading the DW position and are not as effective for neuromorphic applications [14]. Indeed, the maximum velocities and minimum required current densities have been reported for the CPP geometry of current injection [42,44–46,48]. However, all these results were obtained for the case of in-plane anisotropy, while PMA may further improve energy efficiency. At the same time, despite the large number of above-mentioned works devoted to domain walls in nanostrips, there is no clear understanding of the DW motion in MTJs upon perpendicular current injection into a ferromagnet with PMA. To date, there has been only one experimental demonstration [14] of DW motion in an MTJ with PMA in the CPP geometry, which encourages detailed numerical and analytical study of the mechanisms and features of DW dynamics.

In this paper, we investigate in detail the DW dynamics induced by the perpendicularly injected spin-polarized current in an MTJ with PMA. We report the results of micromagnetic modeling on the stable DW states in a free layer of various widths. We also study in detail the influence of different polarizer directions and torque types on the DW dynamics conditions and features. The DW steady motion with velocities up to 200 m/s at current densities below 10^6 A/cm^2 is reported. We analyze DW transformation during motion and demonstrate the Walker breakdown for each DW steady-motion regime. Finally, we provide analytical insight that shows good agreement with micromagnetic simulations and helps to analyze the effect of different parameters on the results.

II. SYSTEM AND METHODS

Let us consider an MTJ nanostrip [Fig. 1(a)], which consists of a ferromagnetic polarizer layer, a spacing insulator, and a ferromagnetic free layer with a single domain wall. The following geometrical parameters of MTJ were chosen: free-layer thickness $h = 2.2$ nm, length $L = 5000$ nm, width $w = 10$–300 nm. The magnetic parameters were chosen according to experimental results [14]: uniaxial magnetic anisotropy along the z axis, saturation magnetization $M_S = 1050$ emu/cm^3, anisotropy constant $K = 7 \times 10^6$ erg/cm^3, exchange constant $A = 2 \times 10^{-6}$ erg/cm, damping parameter $\alpha = 0.005$. The magnetization dynamics in a nanostrip can be described by the Landau-Lifshitz-Gilbert equation with an additional term responsible for the spin transfer torque:

$$\dot{\mathbf{M}} = -\gamma \mathbf{M} \times \mathbf{H}_{\text{eff}} + \frac{\alpha}{M_S} \mathbf{M} \times \dot{\mathbf{M}} - \mathbf{T}_{STT}, \qquad (1)$$

where $\mathbf{M}$ is the magnetization vector, γ is the gyromagnetic ratio, α is the Gilbert damping constant, M_S is the saturation magnetization, and $\mathbf{H}_{\text{eff}}$ is the effective field consisting of the magnetostatic, exchange, anisotropy, and demagnetization fields. The spin transfer torque can be written [49–51] as

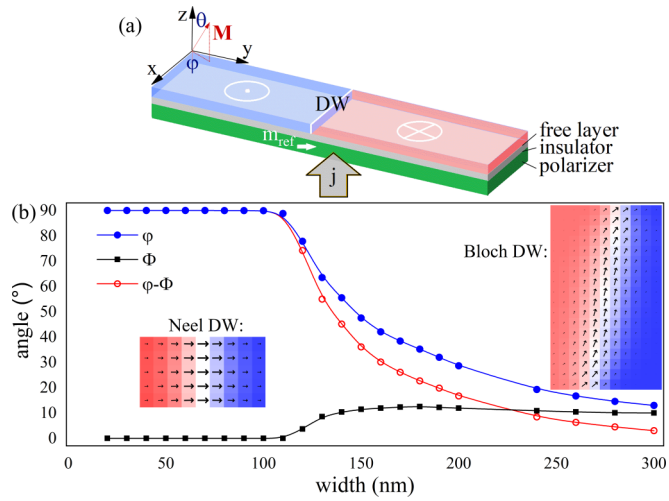

FIG. 1. (a) Schematic representation of the considered MTJ structure with a single domain wall. (b) The dependence of the angles φ between the x axis and the average DW magnetization and Φ between the x axis and the DW plane and their difference in the relaxed state on the MTJ width in the x direction. Inset: Néel and Bloch domain walls. Red and blue correspond to the perpendicular component of $\mathbf{M}$, white is zero, and arrows show the direction and magnitude of planar components.

a sum of two orthogonal components, $\mathbf{T}_{STT} = \mathbf{T}_{ST} + \mathbf{T}_{FLT}$, where the Slonczewski torque (ST) equals $\mathbf{T}_{ST} = -\gamma a_J \mathbf{M} \times [\mathbf{M} \times \mathbf{m}_{\text{ref}}]/M_S$ and the fieldlike torque (FLT) equals $\mathbf{T}_{FLT} = -\gamma b_J [\mathbf{M} \times \mathbf{m}_{\text{ref}}]$. Here, $\mathbf{m}_{\text{ref}}$ is a unit vector along the magnetization direction of the polarizer layer; $a_J \approx \hbar j P/(2heM_S)$, where h is the thickness of the free layer, $\hbar$ is the reduced Planck constant or Dirac constant, j is the current density, $e > 0$ is the charge of the electron, and $P = 0.4$ is the spin polarization of the current; $b_J = \xi_{CPP} a_J$, where ξ_{CPP} is taken to be about 0.4 [45].

Micromagnetic simulations consisting of Eq. (1) numerical integration on a 2×2 nm rectangular grid were performed using our SPINPM micromagnetic finite-difference code based on the fourth-order Runge-Kutta method with adaptive time step control for time integration. To focus on the effect of the spin-polarized current, we ignored the Dzyaloshinskii-Moriya interaction, Oersted fields, and thermal fluctuations.

III. MODELING RESULTS AND DISCUSSION

First of all, micromagnetic modeling of relaxation in a free layer with a single DW was carried out for different widths. One can relate DW evolution from Néel to Bloch type to the magnitude of φ, which is the angle between the x axis and the average DW magnetization in the relaxed state. The Néel domain wall corresponds to $\varphi = 90°$, and the Bloch wall corresponds to $\varphi = 0°$. The range of φ values from 90° to 0° corresponds to the hybrid state of the DW. The dependence of the angle φ on the free-layer width in the x direction is illustrated in Fig. 1(b). For widths up to 110 nm, the magnetization relaxes to the Néel DW, for a width of more than 110 nm, the wall becomes a hybrid, and for a width above 300 nm, the Bloch-type DW is an equilibrium state. These results are consistent with an experimental work [14]. Indeed,

TABLE I. Summary of the DW motion (no, no spin current induced DW motion; slow motion, extremely slow DW motion, which can be neglected; fast motion, steady DW motion).

		$\mathbf{m}_{\text{ref}} = (1, 0, 0)$	$\mathbf{m}_{\text{ref}} = (0, 1, 0)$	$\mathbf{m}_{\text{ref}} = (0, 0, 1)$
Néel	$\mathbf{T}_{FLT}$	slow motion	no	fast motion
	$\mathbf{T}_{ST}$	fast motion	no	slow motion
Bloch	$\mathbf{T}_{FLT}$	no	slow motion	fast motion
	$\mathbf{T}_{ST}$	no	fast motion	slow motion

although DW magnetization at widths of about 300 nm is not parallel to the x axis, the DW plane also has a certain tilt at an angle Φ from the x axis; therefore, the type of DW should be defined by the difference $\varphi - \Phi$, which is almost zero for the mentioned widths. The reason for the tilt of the DW plane is a rather strong magnetostatic field. Our simulation demonstrates that at half the saturation magnetization, the DW plane is perfectly aligned with the x axis, and the Bloch-type DW becomes stable at widths of about 150 nm. It is also possible to avoid this tilt by designing a low magnetostatic shape, for example, with the half-ring geometry, as in [45].

To identify the conditions for DW motion in the outlined MTJ structure, we studied the effect of the spin current while taking into account $\mathbf{T}_{ST}$ and $\mathbf{T}_{FLT}$ separately. We chose 50- and 300-nm-wide nanostrips (with Néel and Bloch initial DWs in a free layer, respectively) as the system for the study. For each geometry, we considered a polarizer magnetized in the x, y and z directions. Thus, six configurations (three polarizations and two torques) for each DW type (width) were considered (see Table I) .

Let's start with planar polarizers. In the case of $\mathbf{m}_{\text{ref}} = (1, 0, 0)$, a Bloch-type DW cannot be excited by either $\mathbf{T}_{ST}$ or $\mathbf{T}_{FLT}$. A Néel-type DW starts a considerably fast steady motion with $\mathbf{T}_{ST}$ action. However, $\mathbf{T}_{FLT}$ also leads to the Néel DW steady motion, but the velocity in this case is extremely low (< 1 m/s). The origin of such DW behavior will be explained later. In the case of $\mathbf{m}_{\text{ref}} = (0, 1, 0)$ we have the opposite situation: a Néel-type DW cannot be excited by either $\mathbf{T}_{ST}$ or $\mathbf{T}_{FLT}$, while a Bloch-type DW demonstrates a considerably fast steady motion under the action of $\mathbf{T}_{ST}$ and an extremely slow steady motion under $\mathbf{T}_{FLT}$ action. It is worth noting that in both no-motion cases, the corresponding $\mathbf{m}_{\text{ref}}$ directions are parallel to the DW magnetization in the DW core, and the vector product of the torques is zero.

In the case of a perpendicular polarizer [$\mathbf{m}_{\text{ref}} = (0, 0, 1)$], both initial DW types start very slow (< 1 m/s) steady motion under the action of $\mathbf{T}_{ST}$. At the same time, $\mathbf{T}_{FLT}$ induces steady motion of significant velocity for both initial DW types.

As seen from Table I, four steady-motion configurations were observed: $\mathbf{T}_{ST}$ excitation with $\mathbf{m}_{\text{ref}} = (1, 0, 0)$ for Néel and $\mathbf{m}_{\text{ref}} = (0, 1, 0)$ for Bloch and $\mathbf{T}_{FLT}$ excitation with $\mathbf{m}_{\text{ref}} = (0, 0, 1)$ for both DW types. Now let's focus on DW dynamics in these torque and polarizer configurations. In all these cases, after the DW motion is initiated by the spin current, which reaches its amplitude instantaneously, φ starts to tilt gradually during the acceleration of the DW until the steady-motion regime is reached and the DW is transformed into a hybrid-type DW [see, for example, Fig. 2(a)]. Thereafter, the DW continues its steady motion with constant φ

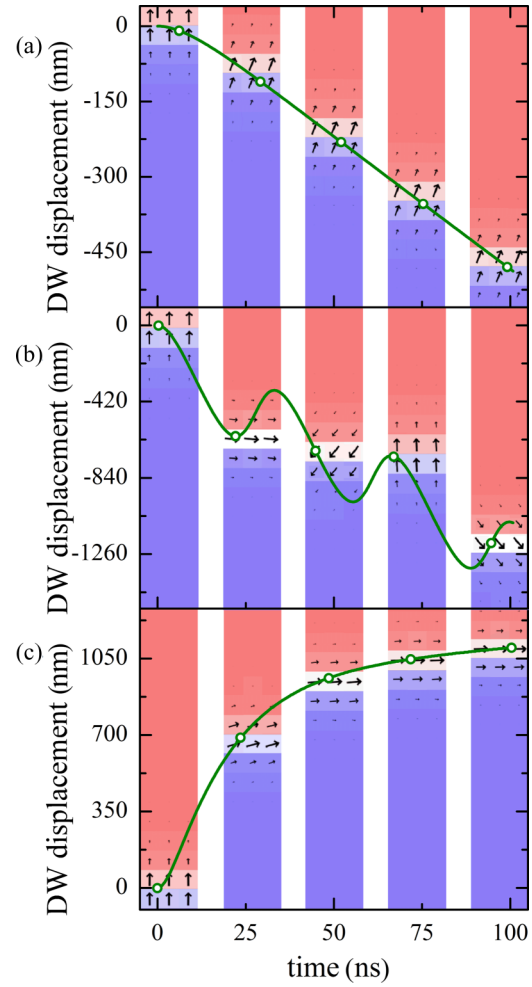

FIG. 2. Displacement of the Néel DW (70 nm wide) vs time in the case of (a) steady motion before Walker breakdown for $j = 0.04 \times 10^6$ A/cm^2 (in the case of a perpendicular polarizer), (b) oscillatory DW motion after Walker breakdown for $j = 0.9 \times 10^6$ A/cm^2 (in the case of a perpendicular polarizer), and (c) DW shift and stop after Walker breakdown for $j = 1.2 \times 10^6$ A/cm^2 (in the case of a planar polarizer).

until it reaches the edge of the nanostrip. It is worth noting that planar and perpendicular polarizers induced motion in opposite directions, which will be explained by the analytical model later. With an increase in the current density, the steady-motion velocity and φ also increase until the current density reaches the critical value j_w and Walker breakdown occurs. However, this breakdown has different behavior for planar and perpendicular polarizers. In the case of a perpendicular polarizer, once the critical value j_w is reached, φ begins to change continuously, and the DW starts to oscillate with some average motion along the nanostrip [see, for example, Fig. 2(b)]. For the planar polarizer case [with $\mathbf{m}_{\text{ref}} = (1, 0, 0)$ for Néel DW and $\mathbf{m}_{\text{ref}} = (0, 1, 0)$ for Bloch DW], with an increase in the current density from zero to j_w, the angle φ changed from φ_0 ($\varphi_0 = 0$ for Bloch DW and $\varphi_0 = \pi/2$ for Néel DW) to $\varphi_0 \pm \pi/2$, the DW type is transformed into the opposite one, and the DW stops after a transitional shift [see, for example, Fig. 2(c)]. The difference between Walker breakdowns can be easily explained by comparing the above mentioned behavior

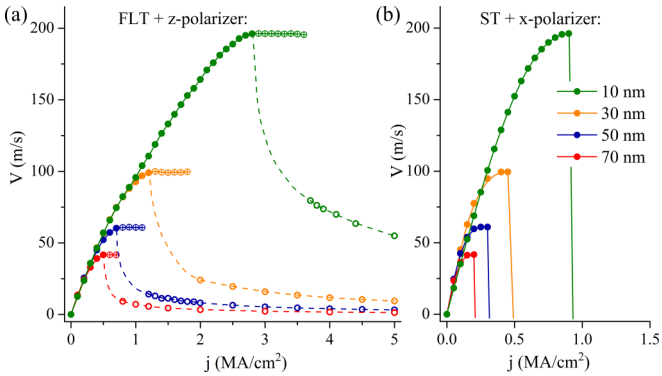

FIG. 3. Average DW's velocity for different widths vs current density for (a) perpendicular polarizer and (b) planar polarizer. Solid lines with solid dots represent steady motion, dashed lines and open dots show averaged motion during oscillations, and crossed dots illustrate post-Walker steady motion caused by magnetostatic stabilization due to the finite size of the nanostrip.

with Table I. Indeed, according to Table I, for a planar polarizer, when DW changes its type to the opposite one, it can no longer be excited by any of the torques. At the same time, for the case of a perpendicular polarizer, motion is excited for both DW types, so the DW continues to move, and φ continues to change, which causes the DW oscillations and its continuous transformation.

Once the symmetries of the components of spin transfer torques ($\mathbf{T}_{STT}$) and the polarizer directions that favor the stable DW motion have been obtained, we proceed with further quantitative analysis. To this end, series of micromagnetic simulations were carried out at various current densities and widths with favorable combinations of polarization and torque. Modeling results demonstrate that DW velocity decreases with increasing DW width. Because of this, here, we display in detail the cases of 10, 30, 50, and 70 nm since for large widths the velocities become too small, although the dependencies remain the same.

The dependences of the average DW velocity, obtained by micromagnetic modeling for the cases of different polarizer directions and nanostrip widths, are shown in Figs. 3(a) and 3(b). The velocity increases with the current density for both planar and perpendicular polarizers [see solid lines with solid dots in Figs. 3(a) and 3(b.)]. At a low current density, it increases almost linearly, and at higher currents, the growth becomes nonlinear, and the velocity tends to saturation. Then, upon reaching the critical current density j_w, Walker breakdown occurs.

In the case of a perpendicular polarizer, above the critical current density j_w, the DW starts to oscillate with some average displacement along the nanostrip. The average motion during these oscillations is shown by the dashed line and open dots in Fig. 3(a). This is not a steady motion, but it is still possible to obtain a certain average velocity which does not depend on the nanostrip length. At the same time, the nanostrip length plays an important role in the case of current densities slightly higher than j_w. In the case of an infinite nanostrip, the DW starts to oscillate immediately after breakdown (see the dashed line), while in the case of a finite nanostrip ($L = 5000$ nm), the DW structure is stabilized due to the magnetostatic interaction near the edge of the nanostrip. Indeed, at current densities slightly higher than j_w, DW tends to make one oscillation before reaching the nanostrip edge, so DW should stop and then change the velocity direction for the first time somewhere near the edge. At the same time, micromagnetic modeling demonstrates that the magnetostatic interaction prevents this stopping and subsequent velocity direction change, as it tries to expel DW from the nanostrip in the region near the edge. This leads to additional steady motion above the Walker breakdown [see crossed dots in Fig. 3(a)] for finite-size samples. Our simulation demonstrates that the range of this post-Walker steady motion decreases with an increase of length L.

In the case of a planar polarizer [Fig. 3(b)] we observe a different behavior. Here, when the DW reaches its maximum velocity at the critical current density j_w, it transforms into another type DW and then stops. However, this transitional process of acceleration and deceleration requires a certain time, during which the DW manages to shift significantly (up to several thousand nanometers in our case) or even to reach the edge of the nanostrip. A similar behavior of DWs in short nanostrips above the Walker breakdown was observed in [46]. Here, we managed to achieve the DW steady-motion velocities up to 200 m/s at current densities below 10^6 A/cm^2. It is important to note that although these low levels of current density may become relatively close to the noise level, they are similar to those used experimentally in a similar DW-based system [14], which makes them feasible. However, in future experiments, one should be aware of the possibility to encounter noise-related problems.

The symmetry of torque considered in this work, in principle, can be obtained not only in the case of CPP injection. In the first approximation, the cases of a planar polarizer are similar to spin-orbit torques [23]. In this regard, the direction of the polarizer can be associated with the direction of polarization of the current in the spin-orbit layer, and ST and FTL can be associated with the spin Hall and direct Rashba effects, respectively. With this in mind, one can find a perfect correlation between Table I and the DW motion conditions in the case of spin-orbit excitation [24]. The dependence of the velocity on the current density for the spin-orbit case and CPP injection case with a planar polarizer is also rather close. At the same time, the effect of the perpendicular polarizer and the corresponding torque symmetry cannot be achieved by the spin-orbit effect due to in-plane polarization of the carriers. This makes the perpendicular polarizer a unique condition for only CPP injection.

In addition, it should be noted that the case of the perpendicular polarizer is the most important in terms of applications. Indeed, in this case, no one needs additional layers for magnetoresistance-based DW detection since the free layer is perpendicularly magnetized. However, in the case of a planar polarizer and spin-orbit-based excitation, it is necessary to add a perpendicularly magnetized analyzer layer. At the same time, the perpendicular polarizer demonstrates rather high DW velocities. Moreover, in this case, after Walker breakdown, DW oscillation with some mean displacement starts, which makes it possible to use this configuration even at currents exceeding the Walker limit.

TABLE II. Spin transfer torque components in spherical coordinates for x, y, z polarizers.

$\mathbf{m}_{\text{ref}}$	(1,0,0)	(0,1,0)	(0,0,1)
T_θ	$-\gamma a_J \sin\varphi$ $-\gamma b_J \cos\theta\cos\varphi$	$\gamma a_J \cos\varphi$ $-\gamma b_J \cos\theta \sin\varphi$	$\gamma b_J \sin\theta$
T_φ	$\gamma a_J \cos\varphi \sin\theta\cos\theta$ $-\gamma b_J \sin\theta\sin\varphi$	$\gamma a_J \sin\varphi\sin\theta\cos\theta$ $+\gamma b_J \sin\theta\cos\varphi$	$-\gamma a_J \sin^2\theta$

IV. ANALYTICAL MODEL

For analytical insight into DW dynamics in our case, let us consider Eq. (1) in spherical coordinates (θ and φ are the azimuth and polar angles, respectively) with the energy within the framework of a one-dimensional model represented by $\varepsilon = \varepsilon_{\text{exch}} + \varepsilon_{\text{magn}} + \varepsilon_{\text{an}} + \varepsilon_{\text{sh.an.}}$, where exchange energy $\varepsilon_{\text{exch}} = A[(\nabla\theta)^2 + \sin^2\theta(\nabla\varphi)^2]$, A is the exchange constant, magnetostatic energy $\varepsilon_{\text{magn}} = 2\pi\kappa M_s^2 \sin^2\theta\sin^2\varphi$, anisotropy energy $\varepsilon_{\text{an}} = K\sin^2\theta$, K is a constant of perpendicular magnetic anisotropy, and shape magnetic anisotropy energy $\varepsilon_{sh.an.} = -(2\pi - \zeta/2)M_S^2\sin^2\theta$. The parameter $\zeta \ll 1$ describes the difference between the demagnetizing factor in the z direction N_z in the considered case and in the case of an infinite film ($N_z = 4\pi - \zeta$). The parameter κ determines the difference between magnetostatic fields in the cases of a nanostrip and an infinite film. It can be calculated approximately, considering the demagnetization factors and magnetostatic interaction of each domain. However, here, we obtain it more accurately by micromagnetic modeling as $\kappa = |\langle H_{ms}\rangle|/4\pi M_S$, where $\langle H_{ms}\rangle$ is the magnetostatic field distribution from the micromagnetic simulation, which was averaged along the x axis (across the nanostrip). With this in mind, Eq. (1) takes the following form:

$$\begin{aligned}\sin\theta\dot\varphi - \alpha\dot\theta &= -\omega Q\delta_0^2\theta_{yy} + \omega\sin\theta\cos\theta\sin^2\varphi \\ &\quad + \omega Q\delta_0^2\sin\theta\cos\theta(\varphi_y)^2 \\ &\quad + \omega Q\sin\theta\cos\theta + T_\theta, \\ \sin\theta\dot\theta + \alpha\sin^2\theta\dot\varphi &= \omega Q\delta_0^2\sin^2\theta\varphi_{yy} \\ &\quad - \omega\sin^2\theta\sin\varphi\cos\varphi + T_\varphi, \end{aligned} \tag{2}$$

where $\omega = 4\pi\gamma\kappa M_S$, $Q = K_\perp/2\pi\kappa M_S^2$, $\delta_0 = \sqrt{A/K_\perp}$, $K_\perp = K - (2\pi - \zeta/2)M_S^2$. The spin transfer torque components T_θ and T_φ depend on the polarizer direction $\mathbf{m}_{\text{ref}}$ and are summarized in Table II.

Now, let us use a Walker-like assumption. We will look for a solution in the form $\varphi = \varphi(t)$, $\theta = \theta[(y - q(t))/\delta(\varphi)]$, where $\delta(\varphi) = \delta_0/\sqrt{1 + Q^{-1}\sin^2\varphi}$ and $q(t)$ is the position of DW. Under these assumptions Eq. (2) can be reduced to

$$\begin{aligned}\frac{\partial^2\theta}{\partial y^2} - \frac{1}{\delta^2(\varphi)}\sin\theta\cos\theta &= -\frac{1+\alpha^2}{\omega Q\delta_0^2}\sin\theta\frac{\partial\varphi}{\partial t} \\ &\quad - \frac{\alpha}{Q\delta_0^2}\sin\theta\sin\varphi\cos\varphi \\ &\quad + \frac{1}{\omega Q\delta_0^2}\left(T_\theta + \frac{\alpha T_\varphi}{\sin\theta}\right). \end{aligned} \tag{3}$$

The solution to the homogeneous equation corresponding to Eq. (3) in this case is well known and is a kink solution that describes the shape of the domain wall:

$$\theta_0 = 2\arctan\left[\exp\left(\pm\frac{y_0 + y - q(t)}{\delta(\varphi)}\right)\right]. \tag{4}$$

Consider the solution to Eq. (3) to be $\theta = \theta_0 + \theta_1$, where $\theta_1 \ll 1$. Neglecting small values and bearing in mind that $\partial^2\theta_0/\partial y^2 - \sin\theta_0\cos\theta_0/\delta^2(\varphi) = 0$, we can rewrite Eq. (3) as

$$\begin{aligned}&\hat L\theta_1 = f(\theta_0), \quad \hat L = \frac{\partial^2}{\partial y^2} - \frac{\cos 2\theta_0}{\delta^2(\varphi)}, \\ &f(\theta_0) = -\frac{1+\alpha^2}{\omega Q\delta_0^2}\sin\theta_0\frac{\partial\varphi}{\partial t} - \frac{\alpha}{Q\delta_0^2}\sin\theta_0\sin\varphi\cos\varphi \\ &\qquad + \frac{1}{\omega Q\delta_0^2}\left(T_\theta + \frac{\alpha T_\varphi}{\sin\theta_0}\right). \end{aligned} \tag{5}$$

According to the Fredholm alternative, this equation has a solution if and only if the right side $f(\theta_0)$ of the equation is orthogonal to the eigenfunction of operator $\hat L$ with zero eigenvalue, which can be found from the equation $\hat L\theta_1^{(0)} = 0$. For the present problem the required eigenfunction takes the form $\theta_1^{(0)} = \partial\theta_0/\partial y$. Then, considering that $\partial\theta_0/\partial y = \pm\sin\theta_0/\delta(\varphi)$, the solvability condition is

$$\langle\sin^2\theta_0\rangle\left((1+\alpha^2)\frac{\partial\varphi}{\partial t} + \alpha\omega\sin\varphi\cos\varphi\right) = T, \tag{6}$$

where $\langle\cdots\rangle$ means integration over y and $T = \langle T_\theta\sin\theta_0 + \alpha T_\varphi\rangle$ varies for different polarizers. After integration over y, one can obtain

$$2(1+\alpha^2)\frac{\partial\varphi}{\partial t} + 2\alpha\omega\sin\varphi\cos\varphi = \frac{1}{\delta(\varphi)}T_i, \tag{7}$$

where the impact of different polarizer directions T_i has the form

$$\begin{aligned}T_x &= 2\pi\gamma\delta(\varphi)\sin\varphi(-a_J - \alpha b_J), \\ T_y &= 2\pi\gamma\delta(\varphi)\cos\varphi(a_J + \alpha b_J), \\ T_z &= 2\gamma\delta(\varphi)(b_J - \alpha a_J). \end{aligned} \tag{8}$$

Let us now consider the stationary motion of the DW. In this case $\partial\varphi/\partial t = 0$ and Eq. (7) can be solved directly for each polarizer. There are five stationary solutions up to a period:

$$\begin{aligned}&\varphi_{x1} = \arccos\left(\frac{-a_J - \alpha b_J}{H_{Wx}}\right) \text{ at } (a_J + \alpha b_J)^2 < H_{Wx}^2, \\ &\varphi_{x2} = 0, \\ &\varphi_{y1} = \arcsin\left(\frac{a_J + \alpha b_J}{H_{Wy}}\right) \text{ at } (a_J + \alpha b_J)^2 < H_{Wy}^2, \\ &\varphi_{y2} = \pi/2, \\ &\varphi_z = \frac{1}{2}\arcsin\left(\frac{b_J - \alpha a_J}{H_{Wz}}\right) \text{ at } (b_J - \alpha a_J)^2 < H_{Wz}^2, \end{aligned} \tag{9}$$

where $H_{Wx} = H_{Wy} = 4\alpha\kappa M_S$ and $H_{Wz} = 2\pi\alpha\kappa M_S$. To find the velocity of the DW for each φ_i case, recall that $\partial\theta_0/\partial t = \mp V\sin\theta_0/\delta(\varphi)$, which follows from Eq. (4). At the same time, Eq. (4) will be a solution of Eqs. (2) under the following condition: $T_\theta, T_\varphi, \alpha, \partial\phi/\partial t \to 0$. In this case, the second equation

in Eqs. (2) gives $\partial\theta_0/\partial t = -\omega \sin\theta_0 \sin\varphi \cos\varphi$, which leads to the dependence of the velocity on φ:

$$V = \frac{\omega\delta_0 \sin\varphi\cos\varphi}{\sqrt{1+Q^{-1}\sin^2\varphi}}. \tag{10}$$

Using it, the corresponding DW velocities for each solution φ_i are

$$V_{x1} = \frac{\pi\gamma\delta_0}{\alpha} \frac{-(a_J+\alpha b_J)\sqrt{H_{Wx}^2-(a_J+\alpha b_J)^2}}{H_{Wx}\sqrt{1+(QH_{Wx})^{-1}\sqrt{H_{Wx}^2-(a_J+\alpha b_J)^2}}},$$

$$V_{x2} = 0,$$

$$V_{y1} = \frac{\pi\gamma\delta_0}{\alpha}(a_J+\alpha b_J)\sqrt{\frac{H_{Wy}^2-(a_J+\alpha b_J)^2}{H_{Wy}^2+Q^{-1}(a_J+\alpha b_J)^2}},$$

$$V_{y2} = 0,$$

$$V_z = \frac{\gamma\delta_0}{\alpha} \frac{b_J-\alpha a_J}{\sqrt{1+(2Q)^{-1}-(2QH_{Wz})^{-1}\sqrt{H_{Wz}^2-(b_J-\alpha a_J)^2}}}. \tag{11}$$

It should be noted that the V_{x1} case is in good agreement with the analytical results for spin Hall effect induced DW motion, analyzed in [27]. This correlates with the similarity in symmetry between the spin Hall effect and the Slonczewski torque with the x-axis polarizer.

Taking into account that α is small and only the term with the torque amplitude (a_J or b_J) without factor α contributes to φ and V significantly [52], these solutions fully correspond to Table I. Indeed, in the case of an x polarizer, there are two solutions: a Bloch DW with zero velocity φ_{x2} and a moving DW, which starts from an ideal Néel DW at zero current and moves with a decrease in φ_{x1} from $\pi/2$ with increasing current until Walker breakdown occurs at $\varphi = 0$ and DW stops. After that, the DW becomes an ideal Bloch DW with no motion. In the case of a y polarizer, there are also two solutions: a Néel DW with zero velocity φ_{y2} and a moving DW, which starts from an ideal Bloch DW at zero current and moves with φ_{y1} increasing from $\varphi = 0$ with increasing current until Walker breakdown occurs at $\pi/2$ and the DW stops. After that, the DW becomes an ideal Néel DW with no motion. In both these cases of planar polarizer, the DW moves under the action of the Slonczewski torque, and the contribution of the fieldlike torque is negligible ($a_J \gg \alpha b_J$); however, FLT can lead to ultraslow motion, which was also observed in micromagnetic simulations.

For the z polarizer, both Néel and Bloch DWs begin to move mostly under the action of the fieldlike torque (since $b_J \gg \alpha a_J$ and the Slonczewski torque leads only to ultraslow motion, which also agrees with the modeling results) with φ_z changing with increasing current until Walker breakdown occurs at $\varphi = \pi/4 + \pi n,\ n \in Z$. However, in contrast to the case of planar polarizers, when approaching the Walker limit ($\pi/2$ or 0), the velocity vanishes; here, Walker breakdown occurs at $\varphi = \pi/4$, which corresponds to the maximum velocity according to Eq. (10). Due to this, the DW does not stop in this case but switches to the nonstationary-motion regime. It is also worth noting that the analytical results also demonstrate the opposite direction of DW motion for z and x polarizers, the same as in micromagnetic simulations. This strictly follows from the opposite signs in V_z and V_{x1}.

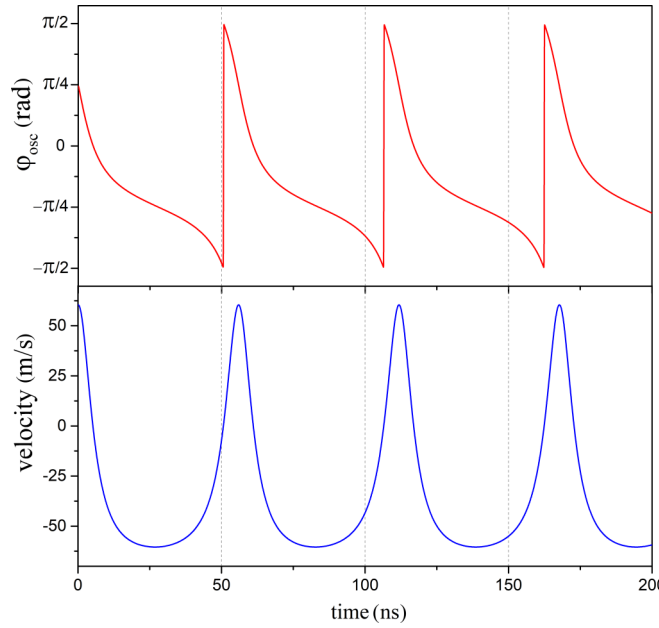

FIG. 4. Dependence of $\varphi_{\rm osc}$ and the corresponding velocity $V_{\rm osc}$ on time for $H_J = 1.2H_{Wz}$ and a nanostrip width of 50 nm, obtained from the equations.

To describe the nonstationary-motion regime, consider Eq. (7). In the case of $(b_J - \alpha a_J)^2 > H_{Wz}^2$ and a z polarizer, this equation can easily be integrated with the initial condition $\varphi(t=0) = \pi/4$ since it is exactly at this angle that the nonstationary regime starts. The resulting dependence of φ above the Walker breakdown, up to a period, is represented by

$$\varphi_{\rm osc} = \arctan\left\{\frac{\sqrt{H_J^2-H_{Wz}^2}}{H_J}\tan\left[\arctan\left(\frac{H_J+H_{Wz}}{\sqrt{H_J^2-H_{Wz}^2}}\right) - \gamma t\sqrt{H_J^2-H_{Wz}^2}\right] - \frac{H_{Wz}}{H_J}\right\}, \tag{12}$$

where $H_J = b_J - \alpha a_J$. Using this and Eq. (10), we can numerically calculate the velocity of the DW above the Walker breakdown. For example, the time dependence of $\varphi_{\rm osc}$ and the corresponding velocity $V_{\rm osc}$ for the case $H_J = 1.2H_{Wz}$ and a nanostrip width of 50 nm is demonstrated in Fig. 4. As can be seen, the analytical model also demonstrates oscillatory motion above the Walker breakdown for the z polarizer, which was observed in micromagnetic modeling. To calculate the average velocity $\langle V_{\rm osc}\rangle$ above the Walker breakdown, this dependence can be averaged.

It is important to note that the one-dimensional model does not take into account some additional magnetization excitations (for example, spin waves, x-axis DW deformations, etc.) considered in micromagnetic modeling. It is, in some aspects, possible to add these excitations indirectly by increasing the damping parameter α since additional excitations lead to

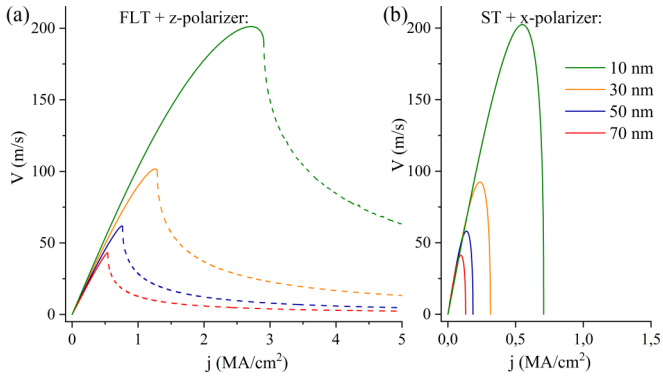

FIG. 5. Analytical dependence of the DW velocity on the current for different polarizer directions and widths (10, 30, 50, and 70 nm). In (a), the solid line corresponds to V_z, and the dashed line corresponds to $\langle V_{\rm osc}\rangle$. In (b), the solid line corresponds to V_{x1}.

additional dissipation. For our analytical results, we increase it to $\alpha = 0.012$ to achieve a better fit with simulations.

A summary of the analytically obtained DW velocity dependence on the current for every polarizer direction and different widths (10, 30, 50, and 70 nm) is presented in Figs. 5(a) and 5(b). In Fig. 5(a) the solid line corresponds to V_z, and the dashed one corresponds to $\langle V_{\rm osc}\rangle$; in Fig. 5(b) the solid line corresponds to V_{x1}. We choose V_{x1}, but not V_{y1}, because for the considered widths we have the Néel DW at zero current, so for the y polarizer we had to take V_{y2}, which is zero. These results show good agreement with micromagnetic simulations (see Fig. 3). This proves the applicability and reliability of the analytical model. However, despite the fact that the analytical solutions perfectly match all regimes (except the post-Walker finite-size steady regime, which obviously cannot be reproduced by the one-dimensional model) and the values of velocities from the micromagnetic modeling, the critical currents differ slightly from the simulation. This is mainly due to the fact that the magnetostatic interaction in the model is rather simplified. As we mentioned earlier, we use the parameter κ, which is obtained from the magnetostatic field distribution. This creates a realistic difference between cases with different widths, and without it the velocities and critical currents would be the same for every width. However, micromagnetic analysis shows that the magnetostatic field, which determines κ, changes during the DW motion with a change in φ. Hence, our estimates of κ for the static DW case give only the correct order for it but not the dependence on the current, which changes the critical currents.

V. CONCLUSIONS

In this paper, we reported a detailed study, both analytically and by micromagnetic modeling, of DW dynamics in a nanostrip with PMA induced by a perpendicularly injected spin-polarized current. The stable DW states depending on the nanostrip width were presented. The influence of different polarizer directions and torque configurations on the dynamics was analyzed in detail. The polarizer and torque configurations at which the steady-state DW motion is feasible were presented. The Walker breakdown was demonstrated, and the dynamics of the postthreshold DW motion was investigated for various configurations of torques and polarizer directions. An analytical model of the system under consideration was proposed and verified by micromagnetic simulations. Our results show the possibility of efficient excitation of DW in nanostripes with PMA with velocities up to 200 m/s at current densities less than 10^6 A/cm^2 in the case of perpendicular current injection. Based on all these, one may expect that the thin-film PMA-based DW spintronic structures will form the basic platform for the next generation of magnetic logic devices, memristors, racetrack memories, etc., possessing a very high energy efficiency.

ACKNOWLEDGMENTS

The work has been supported by the Russian Science Foundation (Project No. 19-12-00432).

[1] G. S. Beach, C. Nistor, C. Knutson, M. Tsoi, and J. L. Erskine, Nat. Mater. **4**, 741 (2005).
[2] J. Grollier, P. Boulenc, V. Cros, A. Hamzić, A. Vaures, A. Fert, and G. Faini, Appl. Phys. Lett. **83**, 509 (2003).
[3] M. Tsoi, R. Fontana, and S. Parkin, Appl. Phys. Lett. **83**, 2617 (2003).
[4] A. Yamaguchi, T. Ono, S. Nasu, K. Miyake, K. Mibu, and T. Shinjo, Phys. Rev. Lett. **92**, 077205 (2004).
[5] Z. Li and S. Zhang, Phys. Rev. B **70**, 024417 (2004).
[6] S. S. Parkin, M. Hayashi, and L. Thomas, Science **320**, 190 (2008).
[7] D. A. Allwood, G. Xiong, C. Faulkner, D. Atkinson, D. Petit, and R. Cowburn, Science **309**, 1688 (2005).
[8] M. Hayashi, L. Thomas, R. Moriya, C. Rettner, and S. S. Parkin, Science **320**, 209 (2008).
[9] J. A. Currivan, Y. Jang, M. D. Mascaro, M. A. Baldo, and C. A. Ross, IEEE Magn. Lett. **3**, 3000104 (2012).
[10] J. A. Currivan-Incorvia, S. Siddiqui, S. Dutta, E. R. Evarts, J. Zhang, D. Bono, C. A. Ross, and M. A. Baldo, Nat. Commun. **7**, 10275 (2016).
[11] X. Wang, Y. Chen, H. Xi, H. Li, and D. Dimitrov, IEEE Electron Device Lett. **30**, 294 (2009).
[12] J. Münchenberger, G. Reiss, and A. Thomas, J. Appl. Phys. **111**, 07D303 (2012).
[13] N. Locatelli, V. Cros, and J. Grollier, Nat. Mater. **13**, 11 (2014).
[14] S. Lequeux, J. Sampaio, V. Cros, K. Yakushiji, A. Fukushima, R. Matsumoto, H. Kubota, S. Yuasa, and J. Grollier, Sci. Rep. **6**, 31510 (2016).
[15] S. Yakata, H. Kubota, Y. Suzuki, K. Yakushiji, A. Fukushima, S. Yuasa, and K. Ando, J. Appl. Phys. **105**, 07D131 (2009).
[16] S. Ikeda, K. Miura, H. Yamamoto, K. Mizunuma, H. Gan, M. Endo, S. Kanai, J. Hayakawa, F. Matsukura, and H. Ohno, Nat. Mater. **9**, 721 (2010).
[17] B. Dieny and M. Chshiev, Rev. Mod. Phys. **89**, 025008 (2017).

[18] D. Ravelosona, D. Lacour, J. A. Katine, B. D. Terris, and C. Chappert, Phys. Rev. Lett. **95**, 117203 (2005).
[19] T. Suzuki, S. Fukami, N. Ohshima, K. Nagahara, and N. Ishiwata, J. Appl. Phys. **103**, 113913 (2008).
[20] M. Yamanouchi, D. Chiba, F. Matsukura, T. Dietl, and H. Ohno, Phys. Rev. Lett. **96**, 096601 (2006).
[21] T. Ono, H. Miyajima, K. Shigeto, K. Mibu, N. Hosoito, and T. Shinjo, Science **284**, 468 (1999).
[22] D. Atkinson, D. A. Allwood, G. Xiong, M. D. Cooke, C. C. Faulkner, and R. P. Cowburn, Nat. Mater. **2**, 85 (2003).
[23] A. Manchon, J. Železný, I. M. Miron, T. Jungwirth, J. Sinova, A. Thiaville, K. Garello, and P. Gambardella, Rev. Mod. Phys. **91**, 035004 (2019).
[24] A. V. Khvalkovskiy, V. Cros, D. Apalkov, V. Nikitin, M. Krounbi, K. A. Zvezdin, A. Anane, J. Grollier, and A. Fert, Phys. Rev. B **87**, 020402(R) (2013).
[25] J. Kwon, S. Goolaup, W. L. Gan, C. H. Chang, K. Roy, and W. S. Lew, Appl. Phys. Lett. **110**, 232402 (2017).
[26] Y. Zhang, S. Luo, X. Yang, and C. Yang, Sci. Rep. **7**, 2047 (2017).
[27] M. Li, J. Wang, and J. Lu, New J. Phys. **21**, 053011 (2019).
[28] N. Sato, K. Schultheiss, L. Körber, N. Puwenberg, T. Mühl, A. A. Awad, S. S. P. K. Arekapudi, O. Hellwig, J. Fassbender, and H. Schultheiss, Phys. Rev. Lett. **123**, 057204 (2019).
[29] T. Taniguchi, J. Grollier, and M. D. Stiles, Phys. Rev. Applied **3**, 044001 (2015).
[30] M. Kläui, P.-O. Jubert, R. Allenspach, A. Bischof, J. A. C. Bland, G. Faini, U. Rüdiger, C. A. F. Vaz, L. Vila, and C. Vouille, Phys. Rev. Lett. **95**, 026601 (2005).
[31] M. Hayashi, L. Thomas, C. Rettner, R. Moriya, Y. B. Bazaliy, and S. S. P. Parkin, Phys. Rev. Lett. **98**, 037204 (2007).
[32] D. Ravelosona, S. Mangin, J. A. Katine, E. E. Fullerton, and B. D. Terris, Appl. Phys. Lett. **90**, 072508 (2007).
[33] Y. B. Bazaliy, B. A. Jones, and S.-C. Zhang, Phys. Rev. B **57**, R3213(R) (1998).
[34] G. Tatara and H. Kohno, Phys. Rev. Lett. **92**, 086601 (2004).
[35] Z. Li and S. Zhang, Phys. Rev. Lett. **92**, 207203 (2004).
[36] S. Zhang and Z. Li, Phys. Rev. Lett. **93**, 127204 (2004).
[37] A. Thiaville, Y. Nakatani, J. Miltat, and Y. Suzuki, Europhys. Lett. **69**, 990 (2005).
[38] A. Mougin, M. Cormier, J. Adam, P. Metaxas, and J. Ferré, Europhys. Lett. **78**, 57007 (2007).
[39] P. J. Metaxas, J. P. Jamet, A. Mougin, M. Cormier, J. Ferré, V. Baltz, B. Rodmacq, B. Dieny, and R. L. Stamps, Phys. Rev. Lett. **99**, 217208 (2007).
[40] S.-W. Jung, W. Kim, T.-D. Lee, K.-J. Lee, and H.-W. Lee, Appl. Phys. Lett. **92**, 202508 (2008).
[41] S. Emori and G. S. Beach, Appl. Phys. Lett. **98**, 132508 (2011).
[42] A. V. Khvalkovskiy, K. A. Zvezdin, Ya. V. Gorbunov, V. Cros, J. Grollier, A. Fert, and A. K. Zvezdin, Phys. Rev. Lett. **102**, 067206 (2009).
[43] C. T. Boone, J. A. Katine, M. Carey, J. R. Childress, X. Cheng, and I. N. Krivorotov, Phys. Rev. Lett. **104**, 097203 (2010).
[44] P. J. Metaxas, J. Sampaio, A. Chanthbouala, R. Matsumoto, A. Anane, A. Fert, K. A. Zvezdin, K. Yakushiji, H. Kubota, A. Fukushima, S. Yuasa, K. Nishimura, Y. Nagamine, H. Maehara, K. Tsunekawa, V. Cros, and J. Grollier, Sci. Rep. **3**, 1829 (2013).
[45] A. Chanthbouala, R. Matsumoto, J. Grollier, V. Cros, A. Anane, A. Fert, A. V. Khvalkovskiy, K. A. Zvezdin, K. Nishimura, Y. Nagamine, H. Maehara, K. Tsunekawa, A. Fukushima, and S. Yuasa, Nat. Phys. **7**, 626 (2011).
[46] J. Sampaio, S. Lequeux, P. J. Metaxas, A. Chanthbouala, R. Matsumoto, K. Yakushiji, H. Kubota, A. Fukushima, S. Yuasa, K. Nishimura, Y. Nagamine, H. Maehara, K. Tsunekawa, V. Cros, and J. Grollier, Appl. Phys. Lett. **103**, 242415 (2013).
[47] P. N. Skirdkov, K. A. Zvezdin, A. D. Belanovsky, J. Grollier, V. Cros, C. A. Ross, and A. K. Zvezdin, Appl. Phys. Lett. **104**, 242401 (2014).
[48] M. Li, Z. An, and J. Lu, Phys. Rev. B **100**, 064406 (2019).
[49] J. C. Slonczewski, J. Magn. Magn. Mater. **159**, L1 (1996).
[50] S. Zhang, P. M. Levy, and A. Fert, Phys. Rev. Lett. **88**, 236601 (2002).
[51] K. Xia, P. J. Kelly, G. E. W. Bauer, A. Brataas, and I. Turek, Phys. Rev. B **65**, 220401(R) (2002).
[52] Here, we used $\alpha = 0.005$. Such a small value is realistic for fairly good soft magnets. However, in the case of a nanostrip with a large number of defects or high DW pinning, this parameter can be rather high, sometimes even greater than 1. In what follows in the main text, we will consider only the small damping case $\alpha \ll 1$, bearing in mind that if the damping becomes equal to or greater than 1, the contribution of the torques becomes the opposite. Moreover, in the case of a perpendicular polarizer V_z, the damping should exceed only ξ_{CPP} (which is less or even much less than 1) for the Slonczewski torque to make the main contribution to the DW excitation.